Spatial Mutual Information and PageRank-Based Contrast Enhancement and Quality-Aware Relative Contrast Measure

Turgay Celik, *Member, IEEE*

***Abstract*— This paper proposes a novel algorithm for global contrast enhancement using a new definition of spatial mutual information (SMI) of gray levels of an input image and PageRank algorithm. The gray levels are used to represent nodes in PageRank algorithm, and the weights between the nodes are computed according to their dependence and spatial spread over the image, which is quantified by using SMI. The rank vector of gray levels resulted from PageRank algorithm is used in mapping input gray levels to output. The damping factor of the PageRank algorithm is utilized to control the level of perceived global contrast on the output image. Furthermore, a new metric is proposed for image quality-aware relative contrast measurement between input and output images. Experimental results show that the proposed algorithm consistently produces good results.**

***Index Terms*— Contrast enhancement, spatial mutual information, PageRank, quality-aware relative contrast measure.**

I. Introduction

IMAGE contrast enhancement is the process of transforming gray-levels of an input image so that the corresponding output image would be perceived as having higher contrast. It is expected that the intensity differences of pixels in a local neighborhood would be increased as result of a successful contrast enhancement process. Since the perceived contrast is highly subjective, one may need to alter the contrast of an image according to its own perception. To address this need contrast enhancement algorithms are proposed which can be categorized into three major groups according to the type of transformation (or mapping) applied to the gray-levels (or intensities) of an image: 1) local contrast enhancement; 2) global contrast enhancement; and 3) hybrid contrast enhancement.

Local contrast enhancement algorithms directly alter pixel intensities based on their local properties. Usually transform-domain representations are employed for the purpose of intensity manipulation. First a forward transformation on the input image is performed to modify the transform domain coefficients followed by an inverse transformation (or reconstruction) to achieve local contrast enhancement. For this kind of algorithms appropriate settings of the underlying parameters is crucial to avoid the image degradation [1]. There is a wide variety of transformations and among them discrete wavelet transform [2] and discrete cosine transform (DCT) [3], [4] are the most popular ones due to their computational efficiencies.

On the other hand, global contrast enhancement algorithms usually employ a single mapping function to map input gray-levels to output gray-levels. In general the histogram of the input image and a desired histogram are employed to build a mapping function. To this end, global histogram equalization (GHE) is a well-known and widely used contrast enhancement algorithm. GHE achieves input-to-output mapping of gray-levels by matching the cumulative histogram of the input image to the desired cumulative histogram. The desired histogram is assumed to be uniform histogram. This entire process is called as histogram specification. GHE fails in providing an efficient histogram specification which is solved by exact histogram specification [5] which guarantees that output image's histogram is approximately same with the desired one.

GHE efficiently utilizes available dynamic range, but will over-enhance output image when there are large peaks in the input histogram. Further, due to floating point operations used in histogram specification it can not guarantee a one-to-one mapping function which results in mapping of the consecutive gray-levels onto the same output gray-level. However, because of its computational efficiency several methods are proposed by modifying either or both the input and desired histograms. Weighted thresholded histogram equalization algorithm (WTHE) [6] clamps the input histogram at an upper and lower thresholds and all the values between these thresholds are transformed using a normalized power law function. The algorithm's performance depends on the thresholds and the power value used. The desired histogram of the brightness preserving histogram equalization with maximum entropy algorithm (BPHEME) [7] has the maximum differential entropy obtained using a variational approach under the mean brightness constraint. Although entropy maximization corresponds to contrast stretching to some extent, it does not always achieve contrast enhancement [8]. In flattest histogram specification with accurate brightness preservation algorithm (FHSABP) [8], convex optimization is used to transform the input histogram into the flattest histogram, subject to a mean brightness constraint. An exact histogram specification method is used to preserve the image brightness. However, when the gray-levels of the input image are uniformly distributed,

Manuscript received February 17, 2016; revised June 28, 2016; accepted July 30, 2016. Date of publication August 9, 2016; date of current version August 23, 2016. The associate editor coordinating the review of this manuscript and approving it for publication was Prof. Damon M. Chandler.

The author is with the School of Computer Science and Applied Mathematics, University of the Witwatersrand, Johannesburg 2000, South Africa, and also with the Signal Processing Group, Bilkent University, Ankara 6800, Turkey (e-mail: celikturgay@gmail.com).

Color versions of one or more of the figures in this paper are available online at http://ieeexplore.ieee.org.

Digital Object Identifier 10.1109/TIP.2016.2599103

FHSABP performs very similar to GHE. Furthermore, it is designed to preserve the average brightness which may produce low contrast results when the average brightness is either too low or too high. Histogram modification framework (HMF) [9] minimizes a parametrized cost function to compute the desired histogram. The cost function is composed of penalty terms of minimum histogram deviation from the input and uniform histograms and histogram smoothness. Furthermore, the edge information is also embedded into the cost function to weight pixels around region boundaries to address noise and black/white stretching. Similar to WTHE, adaptive gamma correction with weighting distribution algorithm (AGCWD) [10] modifies the input histogram by weighting distribution and enhances image automatically by using gamma correction. However, the algorithm may result in the loss of details on bright regions of image if there are high peaks in the input histogram. Further, in order to achieve brightness preservation, the algorithm limits the transformed image's dynamic range to the largest gray-level value of input image which results in limited contrast on the output image. In [11], the discrete histogram of an image is transformed to continuous distribution with Gaussian mixture model (GMM) and the components of the final GMM is used to obtain subregions of the input histogram. A non-linear mapping is further applied to each subregion to find the final transformation. This process may result in improved perceived contrast, however, it is computationally demanding because of parameter estimation process of GMM.

All the above algorithms employ one-dimensional (1D) histogram in their process which is highly sensitive to the peaks. In order to utilize contextual information around each pixel to alleviate the drawbacks of 1D histograms, global contrast enhancement algorithms based on two-dimensional (2D) histograms are proposed [12]–[14]. The two-dimensional histogram equalization algorithm (2DHE) [12] forms a 2D input histogram from the weighted co-occurrences of gray-levels on local neighborhoods of pixels. The diagonal elements of the 2D input histogram is mapped to the diagonal elements of the 2D uniform histogram. Later, contextual and variational contrast enhancement algorithm (CVC) [13] is proposed to improve 2DHE. CVC computes a smooth 2D desired histogram by minimizing the parametrized sum of Forbenius norms of the differences from the 2D input histogram and the 2D uniform histogram. The diagonal elements of the 2D input histogram is mapped to the diagonal elements of the 2D desired histogram to achieve contrast enhancement. This method is further improved by minimizing a complex objective function which considers different factors of the image at the expense of higher computational cost [14]. Compared with the methods employing only 1D histogram, 2D histogram based methods [12]–[14] generally produce outputs with less visual distortions on them. However, to construct a 2D histogram is typically computationally demanding, whose complexity will exponentially increase with an increase of the size of neighborhood considered in forming 2D histogram [13].

The perceived contrast of an image is unified perception of both local and global contrasts. To achieve this a hybrid contrast enhancement algorithm [15] which combines both local and global processes together is proposed. Spatial entropy-based contrast enhancement (SECE) in DCT (SECEDCT) algorithm [15] performs global contrast enhancement (SECE) by mapping each input gray-level to an output gray-level using a weight vector computed from a new definition of spatial entropy of gray-levels. This weight for each gray-level is calculated using spatial entropy normalized by spatial entropies of other gray-levels. Because of this normalization, the global contrast on output image has slightly improved contrast with respect to the input image. Furthermore, SECE does not consider the spatial relationships of gray-levels, hence, most of the time output is simply linear mapping of the input gray-levels. The global contrast enhanced image is further processed by linearly weighing the transform domain coefficients to achieve local contrast enhancement. SECEDCT does not allow to change the level of global contrast, but the level of local contrast. Later, residual spatial entropy-based contrast enhancement (RSECE) is proposed to improve SECE by learning a desired function utilizing both spatial-relationships of gray-levels and controlling the level of global contrast enhancement [16]. Similar to SECEDCT, it is extended to DCT domain (RSECEDCT) to achieve both global and local contrast enhancement. The algorithm attempts to perform average brightness-preservation in DCT domain which makes it computationally demanding. Because of brightness-preservation and histogram specification process, RSECE may not be able to utilize the entire dynamic range which may result in contrast loss on the output image.

In order to address the above mentioned artifacts of RSECE [16], a parametrized global contrast enhancement is proposed in this paper. The gray-levels of the input image are treated as nodes in PageRank algorithm [17]. A weight between two nodes (or between two gray-levels) is computed according to their dependence and spatial spread over the image which is quantified using spatial mutual information (SMI). The output of the PageRank algorithm is used for mapping the input gray-levels to output. The damping factor of the PageRank algorithm is utilized to linearly control the perceived global contrast. SMI quantifies proximity and spatial distribution of two gray-levels over image which is used by PageRank algorithm to allocate larger gaps between consecutive gray-levels with high SMI values which results in higher perceived contrast on the output image. A method to automatically select the control parameter is also introduced. The proposed algorithm is named as *Spatial Mutual Information RANK* (SMIRANK). One can extend SMIRANK to perform both global and local contrast enhancement at the same time using DCT domain coefficients manipulation as in SECEDCT or RSECEDCT. In order to quantify the level of contrast change between the original and processed images, this paper also proposes a new quality-aware relative contrast measure.

The remainder of the paper is organized as follows. The proposed quality-aware relative contrast measure is introduced in Section II. Section III presents the proposed contrast enhancement algorithm. Section IV presents qualitative and quantitative comparisons of the proposed algorithm with

state-of-the-art contrast enhancement algorithms. Section V concludes the paper.

II. Quality-Aware Relative Contrast Measure

Although it is not easy to quantitatively measure the level of perceived contrast, several metrics [3], [15], [18] have been proposed. In general, statistical measures collected from functions of minimum and maximum signal levels within image blocks [3], [15], [18] are used. Thus, one can measure contrast levels of input (original) and processed (output) images separately to quantitatively asses the level of contrast change [15]. Although this may produce statistically relevant results, results mainly depend on the size of image block used for collecting statistics, and ignore the level of deformations on the output image due to enhancement process. Recently, brightness-aware relative contrast measurement (BRCM) is proposed to asses the performance of contrast enhancement process in terms of average brightness preservation and relative contrast change [16]. However, BRCM is not able to assess the level of visual deformations on the output image. It measures the mean of projected gradient difference between original and processed images which may produce incorrect measurement results on images highly distorted due to enhancement process for which relative contrast measure would be measured high but not the visual quality.

In order to address these problems, a quality-aware relative contrast measure (QRCM) is proposed in this paper. This measure considers both the level of relative contrast enhancement between input and output images and distortions resulting from the enhancement process. The measure produces a number in the range $[-1, 1]$ where -1 and 1 refer to full level of contrast degradation and improvement, respectively. QRCM employs the gradient magnitudes of original and processed images to measure the relative contrast change and image quality degradation.

Let $\mathbf{G}_\mathbf{X} = \sqrt{\mathbf{X}_x^2 + \mathbf{X}_y^2}$ be the gradient magnitude map of a 2D image $\mathbf{X}$ computed using the spatial derivative images $\mathbf{X}_x$ and $\mathbf{X}_y$ along x- and y-spatial directions, respectively. The derivative images along x- and y-spatial directions are estimated by first average filtering with a 3×3 box kernel followed by filtering with 3×3 Prewitt kernels [19].

Let $\mathbf{G}_\mathrm{o}$ and $\mathbf{G}_\mathrm{p}$ be the gradient magnitude maps of original ($\mathbf{X}_\mathrm{o}$) and processed ($\mathbf{X}_\mathrm{p}$) images, respectively. The perceived level of contrast is correlated to the magnitude of the gradient. The relative gradient magnitude change between the original and processed images is measured according to

$$\mathbf{G}_{\mathrm{p,o}}(i, j) = \frac{\mathbf{G}_\mathrm{p}(i, j) - \mathbf{G}_\mathrm{o}(i, j)}{\mathbf{G}_\mathrm{p}(i, j) + \mathbf{G}_\mathrm{o}(i, j) + \epsilon}, \tag{1}$$

where (i, j) is pixel spatial location, ϵ is an arbitrarily small number to prevent division by zero. In the case of contrast increase the difference between local pixel intensities increases (so does the magnitude of the gradient), thus the relative gradient magnitude change $\mathbf{G}_{\mathrm{p,o}}$ becomes positive and approaches to 1, and vice versa. The gradient magnitude is close to zero on homogeneous image regions and becomes larger on the boundaries. The same trend is valid for $\mathbf{G}_{\mathrm{p,o}}$. Thus using the gradient magnitude map of original image, a weight map $\mathbf{w}_1$ is created according to

$$\mathbf{w}_1(i, j) = \frac{\mathbf{G}_\mathrm{o}(i, j)}{\sum_{\forall k}\sum_{\forall l} \mathbf{G}_\mathrm{o}(k, l)}, \tag{2}$$

which results in high responses around boundaries and approaches to zero on homogeneous regions. Using the relative gradient change map $\mathbf{G}_{\mathrm{p,o}}$ and weight map $\mathbf{w}_1$, the relative contrast measure (RCM $\in [-1, 1]$) is computed according to

$$\mathrm{RCM} = \sum_{\forall i}\sum_{\forall j} \mathbf{G}_{\mathrm{p,o}}(i, j)\, \mathbf{w}_1(i, j). \tag{3}$$

The metric RCM measures the relative contrast change. The metric value approaches to "1" when there is full contrast improvement on the processed image with respect to the original image, and gets closer to "-1" when there is full contrast degradation. If there is no relative contrast change between two images the corresponding RCM value is "0".

The contrast enhancement process may result in visual distortions. In order to quantify the level of distortions we employed gradient magnitude similarity map (**GMS**) [20] between original and processed images computed according to

$$\mathbf{GMS}(i, j) = \frac{2\mathbf{G}_\mathrm{o}(i, j)\,\mathbf{G}_\mathrm{p}(i, j) + T}{\mathbf{G}_\mathrm{o}(i, j)^2 + \mathbf{G}_\mathrm{p}(i, j)^2 + T}, \tag{4}$$

where $T = 255/\sqrt{2}$ is a constant. The gradient magnitude similarity is high when the gradient magnitude values of original and processed images are similar to each other, and vice versa. The image quality (Q $\in [0, 1]$) of enhancement process is measured using average absolute deviation of gradient magnitude similarity map, i.e.,

$$\mathrm{Q} = 1 - \frac{1}{|\mathbf{G}|}\sum_{\forall i}\sum_{\forall j} |\mathbf{GMS}(i, j) - \mu|\, \mathbf{w}_2(i, j), \tag{5}$$

where $|\mathbf{G}|$ is the number of pixels, μ is the average of **GMS**, and $\mathbf{w}_2$ is the weight map computed from $\mathbf{G}_\mathrm{o}$ according to

$$\mathbf{w}_2(i, j) = \frac{1}{1 + \mathbf{G}_\mathrm{o}(i, j)} \tag{6}$$

which is inversely correlated to the gradient magnitude. In other words, the Q value quantifies gradient magnitude changes over homogeneous image regions resulted from enhancement process. The Q value is close to "1" when the visual deteriorations on the processed image is low, and vice versa. This metric is very similar to that of gradient magnitude similarity deviation (GMSD) [21] where the standard deviation of the gradient magnitude similarity map is used to assess the quality between original and processed images.

Using the relative contrast measure (RCM) and the quality measure (Q) between original and processed images, we defined quality-aware relative contrast measure (QRCM $\in [-1, 1]$) according to

$$\mathrm{QRCM} = \begin{cases} \mathrm{RCM} \times \mathrm{Q}, & \mathrm{RCM} \geq 0; \\ (1 + \mathrm{RCM}) \times \mathrm{Q} - 1, & \mathrm{RCM} < 0, \end{cases} \tag{7}$$

which incorporates contrast measure and image quality together as a final measure. QRCM penalizes the contrast

changes when there is a significant difference between the gradients of original and processed images. This, in general, happens when there are visual distortions on the processed image. Thus, QRCM does not only measure the relative change of contrast but also takes the distortion introduced on the processed image relative to the original image into account.

TID2013 image dataset [22] which offers natural images with different types of distortions and corresponding mean opinion scores (MOSs) collected from human subjects is used to evaluate the performance of QRCM in measuring relative contrast change. Thus distortion type of "contrast change" is employed. The dataset offers 5 different levels of contrast change for each of 25 reference images.

The performance of QRCM is evaluated on three aspects of its prediction power [21]: 1) prediction accuracy; 2) prediction monotonicity; and 3) prediction consistency. Let $\mathbf{C}_{\mathrm{m}}$, $\mathbf{C}_{\mathrm{p}}$ and $\mathbf{C}_{\mathrm{s}}$ respectively be the column vectors of measured relative contrast, predicted relative contrast and subjective relative contrast (MOS) on the test image dataset. The logistic regression function of the following form [21] is employed for nonlinear regression

$$\mathbf{C}_{\mathrm{p}} = \beta_1 \left(\frac{1}{2} - \frac{1}{1 + \exp\left(\beta_2 \left(\mathbf{C}_{\mathrm{m}} - \beta_3\right)\right)} \right) + \beta_4 \mathbf{C}_{\mathrm{m}} + \beta_5, \tag{8}$$

where β_ks are fitting parameters. Using the set of $\{\mathbf{C}_{\mathrm{m}}, \mathbf{C}_{\mathrm{s}}\}$ the parameters of the nonlinear regression is learned. The prediction accuracy of $\mathbf{C}_{\mathrm{p}}$ on $\mathbf{C}_{\mathrm{s}}$ is calculated using Pearson linear correlation coefficient (PLCC), i.e.,

$$\mathrm{PLCC}\left(\mathbf{C}_{\mathrm{p}}, \mathbf{C}_{\mathrm{s}}\right) = \frac{\hat{\mathbf{C}}_{\mathrm{p}}^T \hat{\mathbf{C}}_{\mathrm{s}}}{\sqrt{\hat{\mathbf{C}}_{\mathrm{p}}^T \hat{\mathbf{C}}_{\mathrm{p}} \hat{\mathbf{C}}_{\mathrm{s}}^T \hat{\mathbf{C}}_{\mathrm{s}}}}, \tag{9}$$

where the operator $(\cdot)^T$ takes transpose, and $\hat{\mathbf{C}}_{\mathrm{p}}$ and $\hat{\mathbf{C}}_{\mathrm{s}}$ are respectively mean removed vectors of $\mathbf{C}_{\mathrm{p}}$ and $\mathbf{C}_{\mathrm{s}}$. The Spearman rank order correlation coefficient (SROCC) is used to measure the prediction monotonicity between $\mathbf{C}_{\mathrm{m}}$ and $\mathbf{C}_{\mathrm{s}}$ as follows

$$\mathrm{SROCC}\left(\mathbf{C}_{\mathrm{m}}, \mathbf{C}_{\mathrm{s}}\right) = 1 - \frac{6\mathbf{D}^T\mathbf{D}}{|\mathbf{D}|\left(|\mathbf{D}|^2 - 1\right)}, \tag{10}$$

where $\mathbf{D}$ is the rank difference vector between the rank vectors of $\mathbf{C}_{\mathrm{m}}$ and $\mathbf{C}_{\mathrm{s}}$, and $|\mathbf{D}|$ is the number of elements of $\mathbf{D}$. Lastly, the prediction consistency is evaluated using root mean square error (RMSE) between $\mathbf{C}_{\mathrm{p}}$ and $\mathbf{C}_{\mathrm{s}}$ as follows

$$\mathrm{RMSE} = \sqrt{\frac{\left(\mathbf{C}_{\mathrm{p}} - \mathbf{C}_{\mathrm{s}}\right)^T \left(\mathbf{C}_{\mathrm{p}} - \mathbf{C}_{\mathrm{s}}\right)}{|\mathbf{C}_{\mathrm{p}}|}}. \tag{11}$$

The performance of the QRCM is compared with that of GMSD [21], Q (Eq. (5)) and BRCM. The results are shown in Table I. GMSD is a general purpose image quality assessment metric, and on the average it performs well on different types of distortions [21]. It depends on the gradient magnitude similarity, and contrast changes on the dataset are global which makes it difficult for GMSD to capture them. It is worth to mention that Q performs better than GMSD on assessing contrast changes. On the other hand, QRCM and BRCM are highly correlated to human subject assessment of contrast change. Meanwhile, QRCM outperforms all metrics by achieving highest PLCC and SROCC and lowest RMSE. Thus QRCM is used for assessment of contrast enhancement process.

TABLE I

PERFORMANCE COMPARISONS OF DIFFERENT METRICS IN MEASURING RELATIVE CONTRAST CHANGE ON TID2013 IMAGE DATASET

Metric	PLCC	SROCC	RMSE
GMSD	0.28	0.17	1.16
Q	0.55	0.41	1.18
BRCM	0.86	0.85	0.62
QRCM	0.92	0.88	0.47

III. SMIRANK ALGORITHM

A. Gray-Scale Global Contrast Enhancement

1) Problem Definition: Consider an input image as a two-dimensional array of gray-levels, $\mathbf{X} = \{\mathbf{X}(i,j) \mid 0 \le i \le H-1, 0 \le j \le W-1\}$, of size $H \times W$ pixels, where $\mathbf{X}(i,j) \in \left[0, \mathbb{Z}^+\right]$ is gray-level (or intensity) of pixel (i,j) and assume that $\mathbf{X}$ has a dynamic range of $[x_d, x_u]$ where $\mathbf{X}(i,j) \in [x_d, x_u], \forall (i,j)$. The objective of a contrast enhancement algorithm is to generate a naturally looking enhanced image, $\mathbf{Y} = \{\mathbf{Y}(i,j) \mid 0 \le i \le H-1, 0 \le j \le W-1\}$, which has a better perceived contrast quality than that of $\mathbf{X}$. The dynamic range of $\mathbf{Y}$ can be stretched or compressed into the interval $[y_d, y_u]$, where $\mathbf{Y}(i,j) \in [y_d, y_u]$, $y_d < y_u$ and $\{y_d, y_u\} \in \left[0, \mathbb{Z}^+\right]$. In this work, the enhanced image utilizes the entire dynamic range, e.g., for an 8-bit image $y_d = 0$, and $y_u = 2^8 - 1 = 255$.

Let $\mathcal{X} = \{x_1, x_2, \ldots, x_K\}$ be the sorted set of all gray-levels that exist in an input image $\mathbf{X}$, where $x_1 < x_2 < \ldots < x_K$ and K is the number of the distinct gray-levels. After contrast enhancement, each input gray-level x_k is mapped to an output gray-level y_k to produce a sorted list of output gray-levels $\mathcal{Y} = \{y_1, y_2, \ldots, y_K\}$ where $y_1 \le y_2 \le \ldots \le y_K$. Ideally mapping from x_k to y_k is expected to be one-to-one, however, because of limits of the allowed dynamic range and floating point operations on the discrete set, it usually is not one-to-one. Thus, the entropy of output gray-levels is usually lower than that of input gray-levels.

2) 2D Joint-Spatial Histogram: The 2D spatial histogram of the gray-level x_k on the spatial grid of $\mathbf{X}$ is computed as [15]

$$\mathbf{h}_k = \left\{\mathbf{h}_k(m,n) \mid 0 \le m \le M-1, 0 \le n \le N-1\right\}, \tag{12}$$

where $m, n \in \left[0, \mathbb{Z}^+\right]$, $\mathbf{h}_k(m,n) \in \left[0, \mathbb{Z}^+\right]$ is the number of occurrences of the gray-level x_k in the spatial grid located on the image region $\left[m\frac{H}{M}, (m+1)\frac{H}{M}\right] \times \left[n\frac{W}{N}, (n+1)\frac{W}{N}\right]$. The total number of the grids on 2D histogram is MN which is dynamically estimated using the number of distinct gray-levels K and the aspect ratio $r = \frac{H}{W} \approx \frac{M}{N}$, i.e.,

$$N = \lfloor \left(\frac{K}{r}\right)^{1/2} \rfloor, M = \lfloor (Kr)^{1/2} \rfloor, \tag{13}$$

where the operator $\lfloor \cdot \rfloor$ rounds its argument toward the nearest integer. In forming 2D spatial histogram $\mathbf{h}_k$ of gray-level x_k,

the aspect ratio of the original image is preserved on spatial grid. In this way, spatial characteristics of pixels are preserved in forming of 2D spatial histogram.

The 2D histogram entries are further normalized according to

$$\mathbf{h}_k(m,n) \leftarrow \mathbf{h}_k(m,n)/HW, \tag{14}$$

so that

$$\sum_{k=1}^{K}\sum_{m=1}^{M}\sum_{n=1}^{N}\mathbf{h}_k(m,n) = 1. \tag{15}$$

3) Spatial Mutual Information: The joint spatial 2D histogram $\mathbf{h}_{k,l} = \left\{\mathbf{h}_{k,l}(m,n)\right\}$ of gray-levels x_k and x_l, which represents the proportion of occurrences of the gray-levels x_k and x_l on the image region $\left[m\frac{H}{M},(m+1)\frac{H}{M}\right] \times \left[n\frac{W}{N},(n+1)\frac{W}{N}\right]$, is computed as follows [16]

$$\mathbf{h}_{k,l}(m,n) = \min\left(\mathbf{h}_k(m,n), \mathbf{h}_l(m,n)\right). \tag{16}$$

This new definition of joint spatial 2D histogram allows to compute joint spatial statistics of gray-levels in a computationally efficient way.

In order to measure the dependence of gray-levels x_k and x_l and their spatial spread over the image domain, mutual spatial information $I_{k,l}$ is computed according to

$$I_{k,l} = \sum_{m=0}^{M-1}\sum_{n=0}^{N-1}\mathbf{h}_{k,l}(m,n)\log\left(\frac{\mathbf{h}_{k,l}(m,n)}{\mathbf{h}_k(m,n)\,\mathbf{h}_l(m,n)}\right), \tag{17}$$

where log is natural logarithm and $\log(0) = \log(0/0) = 0$. The mutual spatial information $I_{k,l}$ will be high when gray-levels x_k and x_l occur jointly on close spatial regions and spread over the image domain. Thus, one can allocate higher gap between gray-levels y_k and y_l so that the perceived contrast will be high as well.

4) PageRank Algorithm for Ranking: The spatial mutual information between gray-levels x_k and x_l can be employed to measure the dependence of gray-level x_k to all other gray-levels $x_l, \forall l$. This will result in a symmetric 2D matrix representing all dependences between pair-wise gray-levels. This matrix can be used to assign a rank value for each gray-level according to its joint relation with other gray-levels and spread over the spatial domain. In order to find a rank value for each gray-level, we employed the PageRank algorithm [17].

The PageRank algorithm assigns a PageRank score to each one of webpages available on the Internet [17]. The PageRank score of a webpage represents the probability that a random user chooses to view the webpage. The algorithm computes ranking of webpages using PageRank scores. For each pair of different webpages the algorithm places a PageRank score on the corresponding element of a square matrix if there exists a link in between, otherwise it places a zero. The rows and columns of this square matrix represent indexed webpages on the Internet. Then, this square matrix is used to rank the webpages. We adopted the PageRank algorithm to create ranking vector for the gray-levels of the original image. The gray-levels of an input image represent webpages and PageScores (or GrayLevelScores) between different pairs of gray-levels are calculated using mutual spatial information. The ranking vector is later used for mapping input gray-levels to output. In the following, we describe how we adopt the PageRank algorithm.

Let $\mathbf{H} = \{\mathbf{H}(k,l) \mid 1 \le k \le K, 1 \le l \le K\}$ be $K \times K$ "hyperlink matrix" [17] where K represents the number of gray-levels of the input image and $\mathbf{H}(k,l)$ is GrayLevelScore (or PageScore) between gray-levels (or webpages) x_k and x_l. The GrayLevelScore $\mathbf{H}(k,l)$ is computed according to joint spatial spread of the corresponding gray-levels which is measured using mutual spatial information, i.e.,

$$\mathbf{H}(k,l) = I_{k,l}. \tag{18}$$

The GrayLevelScore (or mutual spatial information) $\mathbf{H}(k,l)$ of gray-levels x_k and x_l is high when both gray-levels occur on the same spatial-grids and their joint occurrence is uniformly distributed on spatial domain of the input image. It is worth to note that for each gray-level x_k there exists at least one gray-level x_l for which $\mathbf{H}(k,l) \neq 0$. Thus there will be no need to fix dangling nodes (or dangling gray-levels) problem [17]. A dangling gray-level x_k is identified as the one for which $\mathbf{H}(k,l) = 0, \forall l, l \neq k$.

Let $\mathbf{S}$ be column normalized matrix derived from $\mathbf{H}$ according to

$$\mathbf{S}(k,l) = \frac{\mathbf{H}(k,l)}{\sum_{\hat{k}=1}^{K}\mathbf{H}\left(\hat{k},l\right)}. \tag{19}$$

The $\mathbf{G}$ matrix is defined according to

$$\mathbf{G} = \alpha\mathbf{S} + (1-\alpha)\,\mathbf{1}\mathbf{v}^T, \tag{20}$$

where $\mathbf{1} \in \mathbb{R}^{K\times 1}$ is the column vector of ones and $\mathbf{v} \in \mathbb{R}^{K\times 1}$ is a vector called the "personalization vector", and $\alpha \in [0,1)$ is "damping factor". In this work we set the personalization vector as uniform vector, i.e., $\mathbf{1}^T\mathbf{v} = 1$.

Using $\mathbf{G}$ matrix, the gray-level rank vector $\mathbf{r} \in \mathbb{R}^{K\times 1}$ of gray-levels is computed using eigen analysis. $\lambda = 1$ is the unique and largest eigenvalue of $\mathbf{G}$ [17]. Thus, the eigensystem

$$\mathbf{G}\mathbf{r} = \mathbf{r} \tag{21}$$

has a unique solution, where $\mathbf{r}$ is a column rank vector. One can solve Eq. (21) in two different ways: 1) by an iterative algorithm using the power method [17]

$$\mathbf{r}^{(t)} = \mathbf{G}\mathbf{r}^{(t-1)}, \tag{22}$$

where $\mathbf{r}^{(0)} = \mathbf{v}$ and iterations are continued until a convergence criterion is met, e.g., $||\mathbf{r}^{(t)} - \mathbf{r}^{(t-1)}|| \le \epsilon$; and 2) by solving the linear system of the form

$$(\mathbf{I} - \alpha\mathbf{S})\,\mathbf{r} = (1-\alpha)\,\mathbf{v}, \tag{23}$$

where $\mathbf{I}$ is $K \times K$ identity matrix, $(\mathbf{I} - \alpha\mathbf{S})$ is non-singular, hence Eq. (23) has a unique solution

$$\mathbf{r} = (1-\alpha)\,(\mathbf{I} - \alpha\mathbf{S})^{-1}\,\mathbf{v}, \tag{24}$$

where $(\mathbf{I} - \alpha\mathbf{S})^{-1}$ is the matrix inverse of $(\mathbf{I} - \alpha\mathbf{S})$, and $\mathbf{1}^T\mathbf{r} = 1$.

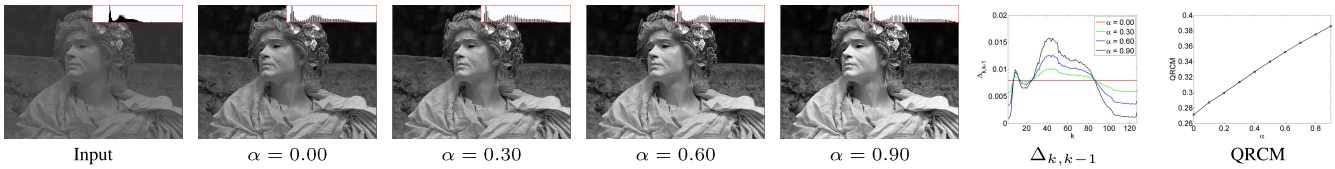

Fig. 1. Sample contrast enhancement results on a test image with "Level 5" contrast degradation from TID2013 image dataset.

5) Mapping Function: Using the rank vector $\mathbf{r}$ the following mapping function is defined to map input gray-levels to output

$$y_k = y_{k-1} + \Delta_{k-1,k}\,(y_u - y_d)\,, \quad \forall k \geq 2 \tag{25}$$

where $y_1 = y_d$, and $\Delta_{k-1,k} \in [0, 1]$ is defined according to

$$\Delta_{k-1,k} = \frac{\mathbf{r}\,(k-1) + \mathbf{r}\,(k)}{2} + \frac{\mathbf{r}\,(1) + \mathbf{r}\,(K)}{2\,(K-1)}, \tag{26}$$

where $\sum_{k=2}^{K} \Delta_{k-1,k} = 1$ (see appendix for proof). The term $\left[\Delta_{k-1,k}\,(y_u - y_d)\right]$ in Eq. (25) is the gap between consecutive output gray-levels y_{k-1} and y_k. This gap is determined according to joint contribution of consecutive gray-levels which is defined as average of their ranks plus the constant $(\mathbf{r}\,(1) + \mathbf{r}\,(K))/(2\,(K-1))$ to ensure that $\sum_{k=2}^{K} \Delta_{k-1,k} = 1$. Note that all output gray-levels are rounded to the nearest integer.

The mapping always guarantees that the minimum and maximum values of output gray-levels are the minimum and maximum values of the allowed dynamic range, i.e., y_d and y_u respectively. Thus, it efficiently utilizes the allowed dynamic range. It is also worth to mention that when $\alpha = 0$, SMIRANK is equivalent to linear stretching.

6) Controlling the Level of Perceived Global Contrast: The proposed algorithm employs α, damping factor, to control the level of perceived global contrast. To demonstrate, a test image with "Level 5" contrast degradation from TID2013 image dataset is selected. The results for different values of α are shown in Fig. 1. Setting $\alpha = 0.0$ is equivalent to linear stretching of gray-levels of the original image which results in minimum level of contrast enhancement. Increasing the value of α also increases the perceived contrast, so does the corresponding QRCM. This is mainly due to the reason that, as can be seen from $\Delta_{k,k-1}$ plots for different values of α, the larger values of α increases the gap from $\Delta_{k,k-1}$ for $\alpha = 0.0$. Meanwhile, contrast increase with larger values of α produces minor distortions on the output image. It is also evident from the histograms of original and processed images that the proposed algorithm preserves the structure of the input histogram. Thus, SMIRANK provides minimum level of information loss.

For an automated process the value of α can be fixed to a default value, e.g. $\alpha = 0.99$ for maximum level of contrast enhancement, or it can be automatically set according to available contrast margin. Here we also propose a method for automatically setting the value of α. The gradient magnitude map $\mathbf{G_X}$ of the input image $\mathbf{X}$ is employed to calculate α according to

$$\alpha = \sum_{\forall i} \sum_{\forall j} \frac{(G_{\mathrm{m}} - \mathbf{G_X}\,(i,j))}{G_{\mathrm{m}}} \mathbf{w}_1\,(i,j)\,, \tag{27}$$

where $G_{\mathrm{m}} = 255\sqrt{2}$ is the maximum gradient magnitude, and $\mathbf{w}_1$ is weight matrix for $\mathbf{G_X}$ as defined in Eq. (2).

B. Color Image Enhancement

The proposed method is designed for gray-scale images, however, it can be easily extended to color images using the following approach [15]. A color image in RGB color space is transformed to HSV color space [19] and the proposed algorithm is only applied on the intensity (or luminance) (V) channel of the transformed image. In order to protect the chrominance information, hue (H) and saturation (S) channels are kept unaltered. This process is followed by an inverse color transformation to reconstruct contrast enhanced color image in RGB color space.

IV. Experimental Results

A. Datasets and Algorithms

We use standard natural test images from TID2013 dataset [22], RGB-NIR dataset [23], and CSIQ dataset [24] for quantitative and qualitative evaluations. The TID2013 image dataset [22] offers 25 reference images of which 24 are natural and 1 is synthetic. Contrast of each reference image is altered at 5 different levels to produce 5 images: "Level 1" corresponds to a small contrast decreasing; "Level 2" corresponds to a small contrast increasing; "Level 3" corresponds to a larger contrast decreasing; "Level 4" corresponds to a larger contrast increasing; and "Level 5" corresponds to the largest contrast decreasing [22]. The RGB-NIR image dataset [23] consists of 477 images in 9 categories captured in RGB and near-infrared (NIR) [23]. RGB images are employed in tests. Similar to TID2013, CSIQ image dataset [24] offers 30 reference images. Contrast of each reference image is degraded at 5 consecutive levels for which "Level 5" corresponds to the largest contrast degrading.

SMIRANK[1] is compared, both quantitatively and qualitatively, with our implementations of GHE, WTHE [6], BPHEME [7], FHSABP [8], HMF [9], CVC [13], 2DHE [12], AGCWD [10], SECE [15], and RSECE [16]. Default parameter settings for all algorithms are used.

B. Quantitative Assessment

The sets of QRCM values $\left\{\mathrm{QRCM}_i^A\right\}_{\forall i}$ computed using all processed images $\left\{\mathbf{Y}_i^A\right\}_{\forall i}$ and corresponding original images $\{\mathbf{X}_i\}_{\forall i}$ are used to statistically determine if contrast enhancement algorithm A satisfies an expected measurement criterion. Two hypotheses are proposed for each criterion:

[1]The MATLAB implementations of SMIRANK and QRCM can be asked from celikturgay@gmail.com with the subject "SMIRANK and QRCM".

TABLE II
THE p-VALUES RESULTING FROM EQ. (29)

Algorithm	TID2013	RGB-NIR	CSIQ
GHE	0.90	0.89	0.97
WTHE	0.97	0.99	1.00
BPHEME	0.87	0.94	0.96
FHSABP	0.87	0.89	0.93
HMF	0.90	0.89	0.98
CVC	0.93	0.99	1.00
2DHE	0.91	0.98	1.00
AGCWD	0.81	0.90	0.71
SECE	0.98	1.00	1.00
RSECE	0.98	0.98	1.00
SMIRANK	1.00	1.00	1.00

null hypothesis H_0 and alternative hypothesis H_1. In order to quantify logical relation ">" between two sets of values $\{\mathrm{T}_i\}_{\forall i}$ and $\{\mathrm{C}_i\}_{\forall i}$ representing test and control sets, respectively, a p value is calculated according

$$p = \frac{\sum_{\forall i} \delta\left(\mathrm{T}_i, \mathrm{C}_i\right)}{\sum_{\forall i} 1}, \tag{28}$$

where $\delta\left(\mathrm{T}_i, \mathrm{C}_i\right) = 1$ if $\mathrm{T}_i > \mathrm{C}_i$, 0 otherwise. The p-value represents the percentage of data points satisfying the logical relation. Using the p-value with the significance level of $p = 0.5$, H_0 is rejected in favor of H_1 if p-value < 0.5.

To test if an algorithm A enhances the contrast of test images, the following hypotheses are tested

$$H_0 : \textbf{A enhances contrast of test images};$$
$$H_1 : \textbf{A does not enhance contrast of test images}, \tag{29}$$

where the null hypothesis H_0 proposes that algorithm A enhances contrast of test images, i.e., $\left\{\mathrm{QRCM}_i^{\mathrm{A}} > 0\right\}$ where $\mathrm{QRCM}_i^{\mathrm{A}}$ is the QRCM value resulted from algorithm A for the input image $\mathbf{X}_i$. The resulting p-values are shown in Table II. On the average, all algorithms manage to satisfy the null hypothesis H_0 of Eq. (29) on all image datasets. However, AGCWD provided the minimum level of enhancement. The results also show that the highest p-values are achieved by SMIRANK. This is mainly due to the reason that, even it is a slight improvement, SMIRANK manages to improve the contrast of all test images regardless the level of contrast margin available on them.

In order to test the relative contrast improvement of an algorithm with respect to other algorithms the following hypotheses are tested

$$H_0 : \textbf{A produces higher contrast wrt B};$$
$$H_1 : \textbf{A does not produce higher contrast wrt B}, \tag{30}$$

where the null hypothesis H_0 proposes that algorithm A produces higher contrast image than that of the algorithm B, i.e., $\left\{\mathrm{QRCM}_i^{\mathrm{A}} > \mathrm{QRCM}_i^{\mathrm{B}}\right\}_{\forall i}$, where $\mathrm{QRCM}_i^{\mathrm{A}}$ and $\mathrm{QRCM}_i^{\mathrm{B}}$ are, respectively, QRCM values resulted from algorithm A and algorithm B for the input image $\mathbf{X}_i$. The resulting p-values are shown in Table III. The results show that AGCWD consistently produces the lowest contrast improvement with respect to the other algorithms. Meanwhile, SMIRANK always produces higher contrast outputs with respect to the other algorithms.

TABLE III
THE p-VALUES RESULTING FROM EQ. (30) ON IMAGE DATASETS WHERE A1 = GHE, A2 = WTHE, A3 = BPHEME, A4 = FHSABP, A5 = HMF, A6 = CVC, A7 = 2DHE, A8 = AGCWD, A9 = SECE, A10 = RSECE AND A11 = SMIRANK

	Alg. B										
Alg. A	A1	A2	A3	A4	A5	A6	A7	A8	A9	A10	A11
A1	–	0.50	0.63	0.71	0.59	0.86	0.54	0.81	0.84	0.54	0.13
A2	0.50	–	0.54	0.60	0.67	0.95	0.54	0.87	0.92	0.46	0.06
A3	0.37	0.46	–	0.74	0.58	0.80	0.50	0.82	0.78	0.53	0.12
A4	0.29	0.40	0.22	–	0.50	0.76	0.41	0.79	0.74	0.36	0.10
A5	0.41	0.33	0.42	0.50	–	0.86	0.46	0.77	0.79	0.45	0.05
A6	0.14	0.05	0.20	0.24	0.14	–	0.09	0.71	0.42	0.06	0.00
A7	0.46	0.46	0.50	0.59	0.54	0.91	–	0.83	0.81	0.38	0.09
A8	0.19	0.13	0.18	0.21	0.23	0.29	0.17	–	0.31	0.11	0.02
A9	0.16	0.08	0.22	0.26	0.21	0.58	0.19	0.69	–	0.09	0.01
A10	0.46	0.54	0.47	0.64	0.55	0.94	0.62	0.89	0.91	–	0.04
A11	0.87	0.94	0.88	0.90	0.95	1.00	0.91	0.98	0.99	0.96	–

TID2013

	Alg. B										
Alg. A	A1	A2	A3	A4	A5	A6	A7	A8	A9	A10	A11
A1	–	0.59	0.56	0.64	0.68	0.66	0.52	0.65	0.74	0.52	0.21
A2	0.41	–	0.45	0.54	0.48	0.72	0.41	0.59	0.87	0.35	0.03
A3	0.44	0.55	–	0.90	0.64	0.61	0.42	0.61	0.78	0.46	0.15
A4	0.36	0.46	0.08	–	0.50	0.52	0.34	0.55	0.69	0.32	0.12
A5	0.32	0.52	0.36	0.50	–	0.62	0.39	0.57	0.73	0.39	0.09
A6	0.34	0.28	0.39	0.48	0.38	–	0.18	0.49	0.79	0.22	0.02
A7	0.48	0.59	0.58	0.66	0.61	0.82	–	0.72	0.86	0.49	0.06
A8	0.35	0.41	0.39	0.45	0.43	0.51	0.28	–	0.65	0.29	0.03
A9	0.26	0.13	0.22	0.31	0.27	0.21	0.14	0.35	–	0.09	0.02
A10	0.48	0.65	0.54	0.68	0.61	0.78	0.51	0.71	0.91	–	0.02
A11	0.79	0.97	0.85	0.88	0.91	0.98	0.94	0.97	0.98	0.98	–

RGB-NIR

	Alg. B										
Alg. A	A1	A2	A3	A4	A5	A6	A7	A8	A9	A10	A11
A1	–	0.35	0.64	0.66	0.66	0.73	0.26	0.95	0.46	0.51	0.24
A2	0.65	–	0.76	0.80	0.81	0.90	0.31	0.98	0.69	0.60	0.20
A3	0.36	0.24	–	0.81	0.43	0.62	0.29	0.92	0.31	0.36	0.15
A4	0.34	0.20	0.16	–	0.41	0.58	0.22	0.90	0.30	0.29	0.13
A5	0.34	0.19	0.57	0.59	–	0.70	0.19	0.96	0.38	0.43	0.12
A6	0.27	0.10	0.38	0.42	0.30	–	0.04	0.99	0.22	0.19	0.08
A7	0.74	0.69	0.71	0.78	0.81	0.96	–	1.00	0.81	0.69	0.32
A8	0.05	0.02	0.08	0.10	0.04	0.01	0.00	–	0.05	0.03	0.00
A9	0.54	0.31	0.69	0.70	0.62	0.78	0.19	0.95	–	0.49	0.16
A10	0.49	0.40	0.64	0.71	0.57	0.81	0.31	0.97	0.51	–	0.12
A11	0.76	0.80	0.85	0.87	0.88	0.92	0.68	1.00	0.84	0.88	–

CSIQ

C. Qualitative Assessment

In this section, a qualitative analysis on color images selected from image datasets enhanced by different algorithms is performed.

The first test image, "Roping", is from CSIQ image dataset [24] which has "Level 1" contrast degradation with respect to the reference image. Contrast enhancement results with corresponding QRCM values and histograms are shown in Fig. 2. The input image has a high dynamic range composed of low- and high-intensity pixels. It is a difficult image for a contrast enhancement algorithm to process. The input image's normalized histogram shows a high peak on a low gray-value. Because GHE performs gray-level mapping between the input and output images by matching cumulative normalized histograms of the input and uniform histograms, the low gray-level is mapped onto a higher gray-level on the output image. This resulted in over-brightening of low-intensity image regions. HMF's weighted average of input and uniform

Fig. 2. Visual and QRCM (in parenthesis) results on "Roping" image with "Level 1" contrast degradation [24].

Fig. 3. Visual and QRCM (in parenthesis) results on "Family" image with "Level 2" contrast degradation [24].

histograms is not able to remove the effect of sharp peak. Hence, the output image is similar to that of GHE. AGCWD's output is similar to that of GHE and HMF with reduced level of over-brightening. Both BPHEME and FHSABP produce output images with lower contrast level than that of the input image. WTHE, CVC and 2DHE slightly improve the contrast without significant visual distortions. Similar to WTHE, CVC, and 2DHE, a slight contrast improvement achieved by SECE and RSECE. Among the contrast enhancement algorithms, SMIRANK achieves the best performance. The output image from SMIRANK has improved visual quality with respect to the input which is also supported by the highest QRCM value.

The second test image, "Family", is from CSIQ image dataset [24] with "Level 2" contrast degradation with respect to the reference image, hence it has a higher margin for contrast improvement with respect to "Level 1" contrast degradation. Contrast enhancement results are shown in Fig. 3. GHE and HMF over-brighten the output image, thus, their contrast improvements are not high. AGCWD has a slight contrast improvement. WTHE, CVC, SECE and RSECE perform well in terms contrast improvement. BPHEME and FHSABP are not able to improve the contrast at all. Indeed FHSABP slightly degrades the contrast on the output image as can be verified by the corresponding negative QRCM value. The best performances among the algorithms are provided by 2DHE and SMIRANK as output image has higher contrast with respect to the input image with no visual distortions and the corresponding QRCM values are highest.

The image "Lake" shown in Fig. 4 has "Level 3" contrast degradation [24]. The histogram of the image shows that pixel intensities are cumulated around mid point of the dynamic range. All algorithms are able to improve the contrast of the input image. However, AGCWD is not able to use the entire dynamic range simply because of the mapping function which maps the maximum value of output gray-levels to the maximum gray-level value in the input image which is 153

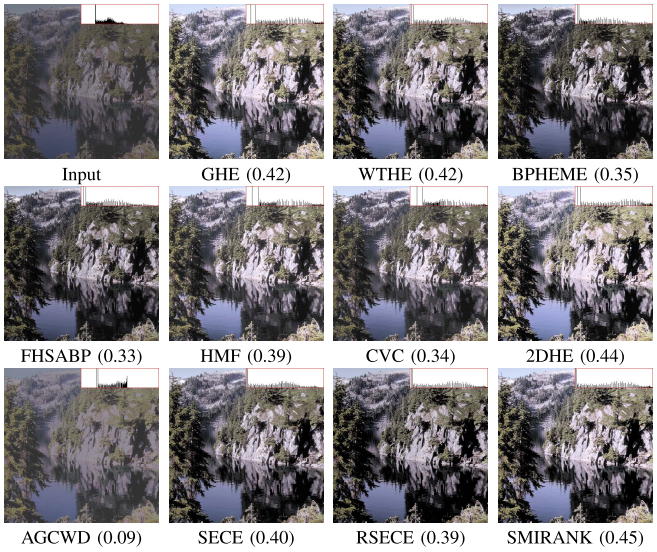

Fig. 4. Visual and QRCM (in parenthesis) results on "Lake" image with "Level 3" contrast degradation [24].

for the image "Lake". It is also clear from the histograms of output images, due to its mapping function SMIRANK efficiently utilizes the entire dynamic range which results in the highest QRCM value. The last test image from CSIQ image dataset [24] is the image "1600" shown in Fig. 5. Its normalized histogram is cumulated around mid-range of the input dynamic range with multiple peaks. All algorithms, except AGCWD, manage to improve the contrast of the input image significantly.

The test image "Water" [23] has fairly uniform normalized histogram stretching over the entire dynamic range as can be seen in Fig. 6. The image has high contrast, and the margin for contrast enhancement is very low. All algorithms manage to produce output images even with slight contrast improvements. One can also notice slight over-brightening over cloud regions on the images from 2DHE and AGCWD. Amongst the algorithms SMIRANK produces the highest

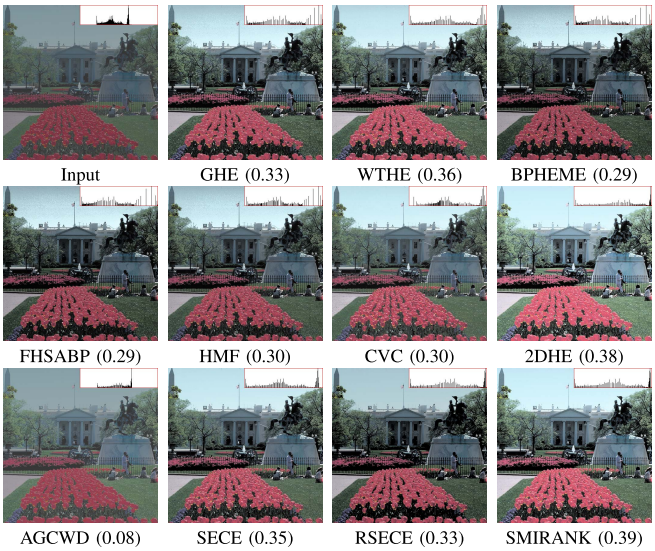

Fig. 5. Visual and QRCM (in parenthesis) results on "1600" image with "Level 4" contrast degradation [24].

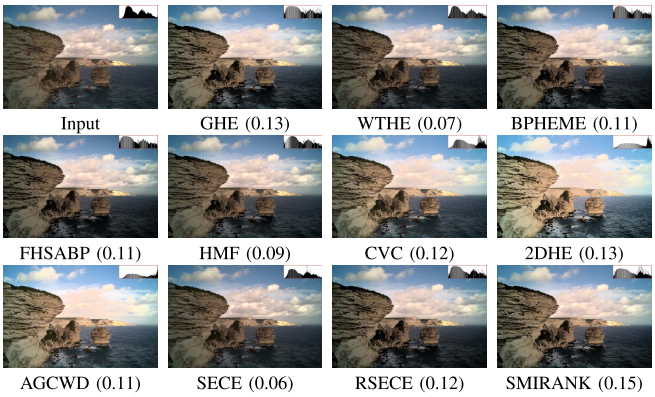

Fig. 6. Visual and QRCM (in parenthesis) results on "Water" image [23].

QRCM value, and a close inspection on the output images also reveals that its output image has slightly higher contrast than that of the other algorithms.

A high contrast image "Urban" [23] is shown in Fig. 7. It has a high-dynamic range comprised of shadow, wall and sky image regions, i.e., gray-levels of the image cumulate around low and high gray-levels. The outputs from GHE, BPHEME, FHSABP, HMF, CVC, 2DHE and AGCWD are over-brightened on shadow regions, which resulted in overall visual quality and contrast loss. WTHE and SECE produce outputs with minor contrast improvements. RSECE and SMIRANK produced the highest contrast enhancement amongst all algorithms.

A low contrast image "Forest" [23] is shown in Fig. 8. Majority of pixel intensities are cumulated around low gray-levels and there are few of them cumulated around high gray-levels. All algorithms except FHSABP significantly improve contrast. It is clear from FHSABP's output that it has lower contrast with respect to the input image which can be verified by negative QRCM value. Highest contrast improvements are achieved by WTHE, HMF and SMIRANK. Meanwhile, HMF's output is slightly over-brightened around center of the image which is not the case for WTHE and SMIRANK.

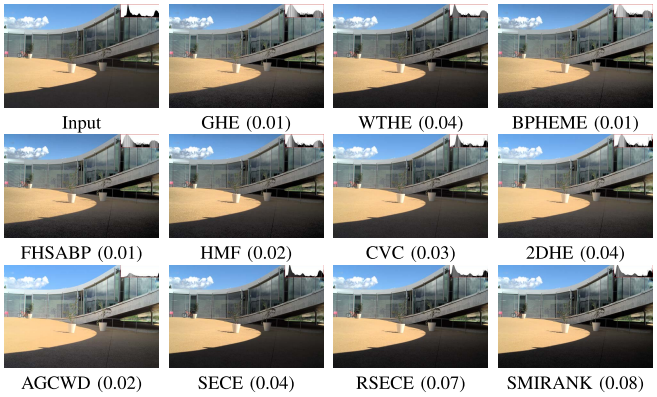

Fig. 7. Visual and QRCM (in parenthesis) results on "Urban" image [23].

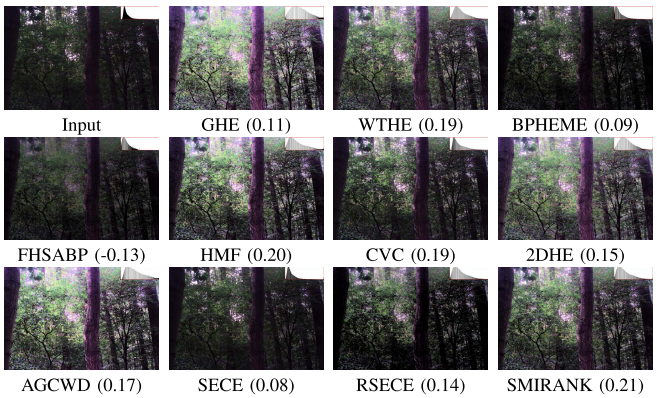

Fig. 8. Visual and QRCM (in parenthesis) results on "Forest" image [23].

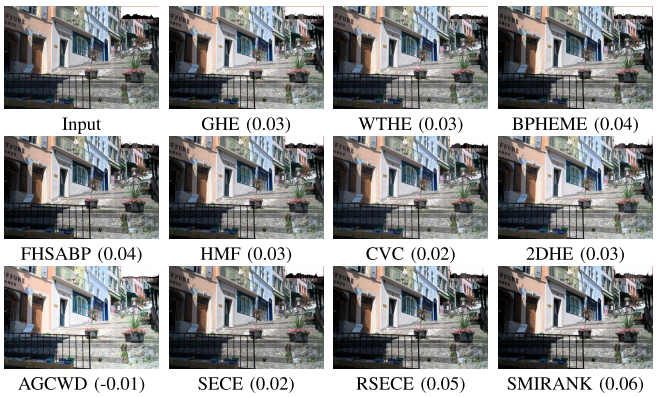

Fig. 9. Visual and QRCM (in parenthesis) results on "Building" image [23].

The last image "Building" [23] is shown in Fig. 9 for which all algorithms except AGCWD perform equally well.

The qualitative and quantitative results show that SMIRANK outperforms all algorithms. Amongst the algorithms performing their operations on spatial histograms, SECE outperformed by RSECE and RSECE is outperformed by SMIRANK. The reason for this is SECE produces outputs very similar to that of linear stretching of gray-levels of the input image. Meanwhile, RSECE produces outputs while tries to preserve average intensity which may result in contrast loss. On the other hand, SMIRANK increases the gap between consecutive gray-levels relatively more if they are spread over the image more than other consecutive gray-level pairs. This process results in increase in perceived level of contrast.

V. Conclusions

A new global contrast enhancement algorithm based on a new definition of spatial mutual information and PageRank algorithm is introduced. The damping factor of the PageRank algorithm is used as parameter to control the level of perceived contrast. It is observed that a linear change of the damping factor value results in a linear change on measured contrast from the output image. Thus, one can linearly control the levels of global contrast changes without significant visual distortions. A method to automatically select the damping factor value is also proposed. Extensive qualitative and quantitative experiments show that the proposed algorithm can achieve contrast improvement on wide-variety of images and produces better or comparable results with respect to existing algorithms. Besides, it can achieve both contrast improvement and image quality preservation at the same time. This makes the proposed algorithm applicable for general purpose contrast enhancement tasks.

In order to measure the relative contrast improvement with respect to a reference image, a quality-aware full-reference contrast metric is also introduced. The metric inherently measures distortions introduced by the contrast enhancement process. It can also measure both contrast improvements and degradations. This new metric highly correlates with mean opinion scores of human subjects.

Appendix

$$\begin{aligned}
\sum_{k=2}^{K}\Delta_{k-1,k} &= \sum_{k=2}^{K}\left(\frac{\mathbf{r}(k-1)+\mathbf{r}(k)}{2}+\frac{\mathbf{r}(1)+\mathbf{r}(K)}{2(K-1)}\right);\\
&= \sum_{k=2}^{K}\frac{\mathbf{r}(k-1)+\mathbf{r}(k)}{2}+\sum_{k=2}^{K}\frac{\mathbf{r}(1)+\mathbf{r}(K)}{2(K-1)};\\
&= \sum_{k=2}^{K}\frac{\mathbf{r}(k-1)}{2}+\sum_{k=2}^{K}\frac{\mathbf{r}(k)}{2}+\sum_{k=2}^{K}\frac{\mathbf{r}(1)+\mathbf{r}(K)}{2(K-1)};\\
&= \frac{1}{2}(1-\mathbf{r}(K)+1-\mathbf{r}(1))+\sum_{k=2}^{K}\frac{\mathbf{r}(1)+\mathbf{r}(K)}{2(K-1)};\\
&= \frac{1}{2}(2-(\mathbf{r}(1)+\mathbf{r}(K)))+\sum_{k=2}^{K}\frac{\mathbf{r}(1)+\mathbf{r}(K)}{2(K-1)};\\
&= 1-\frac{\mathbf{r}(1)+\mathbf{r}(K)}{2}+(K-1)\frac{\mathbf{r}(1)+\mathbf{r}(K)}{2(K-1)};\\
&= 1-\frac{\mathbf{r}(1)+\mathbf{r}(K)}{2}+\frac{\mathbf{r}(1)+\mathbf{r}(K)}{2};\\
&= 1
\end{aligned}$$

References

[1] D. J. Jobson, Z.-U. Rahman, and G. A. Woodell, "A multiscale retinex for bridging the gap between color images and the human observation of scenes," *IEEE Trans. Image Process.*, vol. 6, no. 7, pp. 965–976, Jul. 1997.

[2] R. Fattal, "Edge-avoiding wavelets and their applications," *ACM Trans. Graph.*, vol. 28, no. 3, pp. 1–10, Aug. 2009.

[3] S. S. Agaian, K. Panetta, and A. M. Grigoryan, "Transform-based image enhancement algorithms with performance measure," *IEEE Trans. Image Process.*, vol. 10, no. 3, pp. 367–382, Mar. 2001.

[4] S. S. Agaian, B. Silver, and K. A. Panetta, "Transform coefficient histogram-based image enhancement algorithms using contrast entropy," *IEEE Trans. Image Process.*, vol. 16, no. 3, pp. 741–758, Mar. 2007.

[5] D. Coltuc, P. Bolon, and J.-M. Chassery, "Exact histogram specification," *IEEE Trans. Image Process.*, vol. 15, no. 5, pp. 1143–1152, May 2006.

[6] Q. Wang and R. K. Tan, "Fast image/video contrast enhancement based on weighted thresholded histogram equalization," *IEEE Trans. Consum. Electron.*, vol. 53, no. 2, pp. 757–764, May 2007.

[7] C. Wang and Z. Ye, "Brightness preserving histogram equalization with maximum entropy: A variational perspective," *IEEE Trans. Consum. Electron.*, vol. 51, no. 4, pp. 1326–1334, Nov. 2005.

[8] C. Wang, J. Peng, and Z. Ye, "Flattest histogram specification with accurate brightness preservation," *IET Image Process.*, vol. 2, no. 5, pp. 249–262, Oct. 2008.

[9] T. Arici, S. Dikbas, and Y. Altunbasak, "A histogram modification framework and its application for image contrast enhancement," *IEEE Trans. Image Process.*, vol. 18, no. 9, pp. 1921–1935, Sep. 2009.

[10] S.-C. Huang, F.-C. Cheng, and Y.-S. Chiu, "Efficient contrast enhancement using adaptive gamma correction with weighting distribution," *IEEE Trans. Image Process.*, vol. 22, no. 3, pp. 1032–1041, Mar. 2013.

[11] T. Celik and T. Tjahjadi, "Automatic image equalization and contrast enhancement using Gaussian mixture modeling," *IEEE Trans. Image Process.*, vol. 21, no. 1, pp. 145–156, Jan. 2012.

[12] T. Celik, "Two-dimensional histogram equalization and contrast enhancement," *Pattern Recognit.*, vol. 45, no. 10, pp. 3810–3824, 2012.

[13] T. Celik and T. Tjahjadi, "Contextual and variational contrast enhancement," *IEEE Trans. Image Process.*, vol. 20, no. 12, pp. 3431–3441, Dec. 2011.

[14] C. Lee, C. Lee, and C.-S. Kim, "Contrast enhancement based on layered difference representation of 2D histograms," *IEEE Trans. Image Process.*, vol. 22, no. 12, pp. 5372–5384, Dec. 2013.

[15] T. Celik, "Spatial entropy-based global and local image contrast enhancement," *IEEE Trans. Image Process.*, vol. 23, no. 12, pp. 5298–5308, Dec. 2014.

[16] T. Celik and H.-C. Li, "Residual spatial entropy-based image contrast enhancement and gradient-based relative contrast measurement," *J. Mod. Opt.*, vol. 63, no. 16, pp. 1600–1617, 2016.

[17] P. Berkhin, "A survey on PageRank computing," *Internet Math.*, vol. 2, no. 1, pp. 73–120, Jan. 2005.

[18] K. Panetta, C. Gao, and S. Agaian, "No reference color image contrast and quality measures," *IEEE Trans. Consum. Electron.*, vol. 59, no. 3, pp. 643–651, Aug. 2013.

[19] R. C. Gonzalez and R. E. Woods, *Digital Image Processing*, 3rd ed. Upper Saddle River, NJ, USA: Prentice-Hall, 2006.

[20] A. Liu, W. Lin, and M. Narwaria, "Image quality assessment based on gradient similarity," *IEEE Trans. Image Process.*, vol. 21, no. 4, pp. 1500–1512, Apr. 2012.

[21] W. Xue, L. Zhang, X. Mou, and A. C. Bovik, "Gradient magnitude similarity deviation: A highly efficient perceptual image quality index," *IEEE Trans. Image Process.*, vol. 23, no. 2, pp. 684–695, Feb. 2014.

[22] N. Ponomarenko *et al.*, "Image database TID2013: Peculiarities, results and perspectives," *Signal Process., Image Commun.*, vol. 30, pp. 57–77, Jan. 2015.

[23] M. Brown and S. Süsstrunk, "Multi-spectral SIFT for scene category recognition," in *Proc. Comput. Vis. Pattern Recognit.*, 2011, pp. 177–184.

[24] E. C. Larson and D. M. Chandler, "Most apparent distortion: Full-reference image quality assessment and the role of strategy," *J. Electron. Imag.*, vol. 19, no. 1, pp. 011006-1–011006-21, Mar. 2010.

Turgay Celik received the Ph.D. degree from the University of Warwick, U.K., in 2011. He is a Professor of Computer Science with the University of Witwatersrand. He has been actively reviewing and publishing in various international journals and conferences. He is an Associate Editor of the IEEE Geoscience and Remote Sensing Letters and *Springer Signal, Image and Video Processing Journal*. His research interests include the areas of visual computing, cognitive computing, machine learning, data science, software engineering, and remote sensing.